2014 5th IEEE RAS & EMBS International Conference on
Biomedical Robotics and Biomechatronics (BioRob)
August 12-15, 2014. São Paulo, Brazil

Cascade Robot Force Control Architecture for Autonomous Beating Heart Motion Compensation with Model Predictive Control and Active Observer

Michel Dominici and Rui Cortesão

University of Coimbra, Institute of Systems and Robotics, 3030 Coimbra, Portugal
emails: michel.dominici@gmail.com cortesao@isr.uc.pt

***Abstract*— Nowadays, robotic-assisted surgery does not allow beating heart surgery with autonomous motion compensation functionalities. This paper tackles this problem, based on a robotic control architecture that relies on force feedback. The algorithm merges two cascade loops. The inner one is based on the Kalman active observer (AOB), performing model-reference adaptive control to impose a well-defined stable plant. The outer one, based on a model predictive control (MPC) approach, generates control references for beating heart motion compensation. Two robots are used in the experiments. A lightweight 4-DoF surgical robot generates desired surgical forces and a 3-DoF robot equipped with an ex vivo heart at the end-effector reproduces realistic heart motion. Additionally, robustness to cardiac stiffness mismatches is analyzed.**

I. Introduction

Cardiovascular diseases are the first cause of mortality in the world. More than 17 million people die every year, representing 29% of all global deaths. Among these, coronary heart diseases are the most critical ones, reaching up to 7.2 million deaths [1]. The coronary artery bypass grafting (CABG) is the most common surgical intervention to reduce the risk of death. Currently, the CABG procedure involves a median sternotomy (a $16-20$ [cm] incision in the thorax allowing a direct access to the heart) and a cardiopulmonary bypass (CPB), where heart and lung functionalities are performed by an extracorporal machine. Significant trauma and infection risks due to the long duration of surgery are the major downsides of the sternotomy approach [2], [3]. But the greatest source of complications and post-operatory mortality for patients is due to the CPB. Problems such as inflammatory blood response to the heart-lung machine, the risk of microemboly, kidney dysfunctions and neurological complications such as stroke during the clamping of the aorta have motivated new solutions that circumvent the use of extracorporal circulation [4]. Passive mechanical stabilizers have been conceived for locally decreasing heart motion, allowing direct surgical procedures on the beating heart. Placed around a region of interest (e.g., coronary artery), these stabilizers constraint the motion by suction or pressure. Many improvements have been done over the years, although considerable residual heart motion ($1-1.5$ [mm]) still remains [5]. Additionally, the intense pressure necessary to cancel out heart motion affects blood circulation. Sucker-type stabilizers do not present this problem, but they introduce vacuum pressure that can cause epicardial damage [6]. In this paper we propose force control techniques, which can be applied to robotic-assisted heart surgeries, where autonomous heart motion compensation still remains an issue.

The paper is organized as follows. Related work mainly in the area of beating heart surgery is addressed in Section II. The overall cascade MPC-AOB architecture is presented in Section III where an AOB inner loop guarantees a well defined stable plant and an MPC outer loop compensates force disturbances induced by heart motion. Experimental results with a time varying surgical force reference are presented in Section IV. Finally, Section V concludes the paper.

II. Related work

Compensating physiological motion autonomously through sensory data (e.g., vision and/or force) enables comfortable surgery without the drawbacks of classical procedures, powering and enhancing surgical dexterity. Based on visual servoing and a high speed vision system, Ginhoux and co-authors [7] proposed a motion canceling algorithm based on a MPC approach where future heart motion is predicted. This approach assumes that the heartbeat rate stays constant. More recently, Bachta and co-authors in [8] and [9] improved classical stabilizer solutions with piezo-electrical actuation for a 1 DoF system. Using vision data, H_∞, feedback control with notch filter and MPC are assessed through *in vivo* experiments, requiring prior knowledge of heart motion. Solutions only based on visual servoing present several drawbacks [10]. Surgeries are performed in a cluttered environment where medical instruments can occlude artificial and natural landmarks. This situation entails tracking problems, disturbing motion compensation. Moreover, contact tasks (e.g., suturing, incision and ablation) locally deform soft tissues, affecting landmark calibration. Another important point is that during contact tasks, physiological motion induces disturbance forces which can hardly be compensated by vision information.

Control architectures based on force feedback do not suffer from these drawbacks and can give haptic feedback to surgeons, which is an indispensable feature for surgical telemanipulation, in particular for operations with delicate suture material [11], [12], [13]. However, these architectures have to deal with higher sensor noise (e.g., for low contact forces, the noise is often bigger than the signal) and no physiological motion information can be obtained before contact. Cagneau and co-authors [14] have proposed a force feedback control scheme to compensate the periodic motion of organs. Iterative learning control was implemented as an outer loop to reject periodic disturbances, reducing bad transients during the learning phase. No specific model is necessary for the robot and environment, although the period of the perturbation needs to be known in advance. This assumption is problematic for cardiac surgeries due to random and chaotic nature of heart motion [15]. Cortesão and Poignet [16] have proposed two independent active observers (AOB) for force control and motion compensation. The first AOB is responsible for model-reference adaptive control to guarantee a desired closed loop dynamics for the force. The second one performs control actions to compensate physiological motion. Simulation results have shown high quality compensation capabilities. In [17] Yuen and co-authors proposed a feedforward force controller to compensate force disturbances induced by the mitral valve motion. Using a 3D ultrasound device, the mitral valve motion is estimated and sent to the controller. *In vivo* experiments have shown good capability to maintain in one direction a constant force on the mitral valve. More recently, Kesner and Howe [18] have presented a catheter robotic system dedicated to beating heart surgery. A home made 1-DoF distal force sensor provides force feedback information. Additionally, a force-modulated position controller with friction and dead zone compensation was developed to apply a constant force on the mitral valve. The results showed good capability to maintain in one direction a constant force on a fast moving target, although catheter-based solutions have a limited force range. In [19] we have presented a comparative study of two force control architectures for physiological motion compensation. The first one based on a model predictive control approach uses a mathematical model to predict system behavior [20]. The second one is based on a Kalman active observer to impose desired closed-loop dynamics [21]. The performance of both controllers has been evaluated for constant force references. MPC and AOB have shown good motion compensation capabilities, although residual force amplitudes were still high to consider these architectures without improvements. Therefore, in this paper we intend to merge both MPC and AOB control architectures to achieve better results.

III. MPC-AOB Cascade Control Architecture

The MPC approach presented in [22] is applied to an unstable system. Even if MPC can deal with such plant, a stable plant is more robust to handle external disturbances (such as heart motion). Therefore we merge the classical MPC approach with the AOB design [21] into two cascade loops as shown in Fig. 1. An AOB inner loop is designed to guarantee a well-defined stable plant. The MPC external loop, based on a model of this well-defined stable plant, predicts system behaviors and computes the control reference for the inner loop.

This section is organized as follows. The open loop system plant G_{ol} is described in Section III-A, based on robot dynamics and computed torque techniques. The AOB architecture is addressed in Section III-B, based on a desired closed loop model G_{cl}. The MPC architecture build on top of G_{cl} is presented in Section III-C.

A. Open Loop System Plant

WAM robot dynamic parameters have been identified and used to generate inverse dynamic model (IDM). Computed torque control in the task space is implemented to linearize the WAM robot. Given a set of generalized joint coordinates q describing robot's posture, the well-known robot dynamics is represented by

$$M(q)\ddot{q} + c(\dot{q}, q) + g(q) = \tau, \tag{1}$$

where $M(q)$ is the mass matrix, $c(\dot{q}, q)$ is the vector of Coriolis and centripetal forces, $g(q)$ is the gravity term, and τ is the generalized torque acting on q. Using the operational space formulation, (1) can be written as

$$\Lambda_x(q)\ddot{X} + \Omega_x(q, \dot{q}) = F_c + F_e\,, \tag{2}$$

where X is the Cartesian position, $\Lambda_x(q)$ is the operational space mass matrix, and $\Omega_x(q, \dot{q})$ lumps Coriolis, centripetal, and gravity terms, all in Cartesian coordinates. F_c is the command force and F_e represents external forces acting on the robot end-effector. Knowing robot dynamic parameters and measuring F_e, F_c can be computed by

$$F_c = -F_e + \Lambda_x(q) f^\star + \Omega_x(q, \dot{q})\,, \tag{3}$$

to obtained the decoupled plant

$$\ddot{X} = f^\star. \tag{4}$$

Modeling errors in (3) corrupt (4), motivating the use of the AOB architecture to compensate them. Equation (4) represents the dynamics of a unitary mass. $f^\star$ is an acceleration, being an input parameter. Introducing a damping term K_2 and taking into account the system delay T_d (mainly due to signal processing), as well as a contact model represented by $\hat{K}_s$ (an estimation of the heart stiffness K_s), the linear system plant G_{ol} for each Cartesian dimension is given by

$$G_{ol} = \frac{\hat{K}_s\, e^{-sT_d}}{s(s + K_2\, e^{-sT_d})}\,. \tag{5}$$

For small T_d,

$$G_{ol} \approx \frac{\hat{K}_s\, e^{-sT_d}}{s(s + K_2)}\,. \tag{6}$$

Its equivalent temporal representation is

$$\ddot{y}(t) + K_2\dot{y}(t) = \hat{K}_s v(t - T_d), \tag{7}$$

where $y(t)$ is the plant output (measured force at the robot's end-effector) and $v(t)$ is the plant input which is an acceleration reference. Defining the state variables $x_1(t) = y(t)$

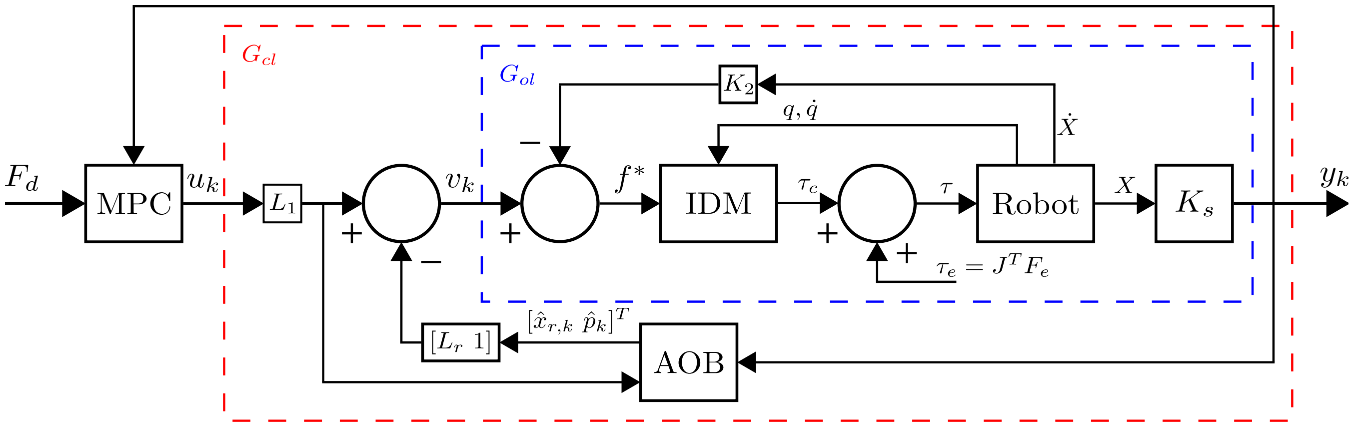

Fig. 1. Cascade MPC-AOB force control architecture for beating heart surgery. Computed torque techniques linked with the robot inverse dynamics model (IDM) generate a decoupled and linearized system. The open loop transfer function G_{ol} also takes into account a damping factor K_2 and the environment stiffness K_s. The desired closed loop transfer function G_{cl} is obtained by the AOB architecture using the state-feedback gain L_r and the extra state $\hat{p}_k$. L_1 is the first element of L_r. The MPC generates a processed reference force u_k for AOB control, based on the desired force F_d, the measured force y_k and G_{cl}. The external torque τ_e is mainly due to beating heart disturbances.

and $x_2(t) = \dot{y}(t)$, (7) can be written as

$$\left[\begin{array}{c} \dot{x}_1(t) \\ \dot{x}_2(t) \end{array} \right] = \left[\begin{array}{cc} 0 & 1 \\ 0 & -K_2 \end{array} \right] \left[\begin{array}{c} x_1(t) \\ x_2(t) \end{array} \right] + \left[\begin{array}{c} 0 \\ \hat{K}_s \end{array} \right] v(t - T_d). \tag{8}$$

Discretizing with sampling time T_s, the equivalent discrete time system is of form[1]

$$\left\{ \begin{array}{lcl} x_{r,k} & = & \Phi_r x_{r,k-1} + \Gamma_r v_{k-1} \\ y_k & = & C_r x_{r,k} \end{array} \right. . \tag{9}$$

In our case, $x_{r,k}$ has dimension three. The first two states of the discretized system represent respectively the end-effector force and its derivative (only the force is measured). The other state is due to system delay $T_d = T_s$ and equal to v_{k-1}.

B. Active Observer Architecture

The continuous plant (6) and its discrete equivalent (9) are unstable due to a pole at the origin. To increase performance and robustness, our model predictive formulation requires a well-defined stable plant. Therefore a first-order active observer is implemented to achieve it. This design is motivated by previous work [24], where a first-order AOB is enough to deal with internal modeling error. The AOB requires the description of the open loop system plant (9) as well as the desired closed loop model G_{cl}. Defining G_{cl} by

$$G_{cl} = \frac{1}{(1 + T_{cl}s)^2} e^{-sT_d}, \tag{10}$$

which corresponds to a critically damped system with time constant T_{cl} where the input is the force reference u_k and the output is the measured force y_k, a state-feedback L_r can be computed in straightforward way. Additionally, one extra state $\hat{p}_k$ is introduced to compensate system disturbances, since a first-order AOB has been chosen [25], [24], [21]. The AOB closed-loop estimation is given by

$$\left[\begin{array}{c} \hat{x}_{r,k} \\ \hat{p}_k \end{array} \right] = \hat{x}_a^- + K_k \left(y_k - \hat{y}_k \right) \tag{11}$$

and

$$\hat{y}_k = \left[\begin{array}{cc} C & 1 \end{array} \right] \hat{x}_a^-, \tag{12}$$

where the *a priori* augmented state estimation $\hat{x}_a^-$ is given by

$$\hat{x}_a^- = \left[\begin{array}{cc} \Phi_r - \Gamma_r L_r & 0 \\ 0 & 1 \end{array} \right] \left[\begin{array}{c} \hat{x}_{r,k-1} \\ \hat{p}_{k-1} \end{array} \right] + \left[\begin{array}{c} \Gamma_r \\ 0 \end{array} \right] u_{k-1}. \tag{13}$$

The Kalman gain K_k reflects uncertainties associated to the system state $\left[\begin{array}{cc} \hat{x}_r(k) & \hat{p}(k) \end{array} \right]^T$, depending on system ($Q_k$) and measurement ($R_k$) noise matrices. Q_k is of form

$$Q_k = \left[\begin{array}{cc} Q_{x_{r,k}} & 0 \\ 0 & Q_{p_k} \end{array} \right]. \tag{14}$$

The absolute values of R_k and Q_k are not important, since only the relative relation is relevant for the Kalman gain [21]. The AOB is inserted in the cascade architecture depicted in Fig. 1. The MPC generates a processed force reference u_k for AOB control, based on the prediction of the overall system dynamics, which includes the desired force F_d, the measured force y_k and G_{cl}.

C. Model Predictive Control Architecture

The MPC is a model based control architecture developed around a finite receding horizon strategy, and it requires a discrete state space model of G_{cl}. From (10), G_{cl} can be represented by

$$\left\{ \begin{array}{lcl} x_k & = & A x_{k-1} + B u_{k-1} \\ y_k & = & C x_k \end{array} \right. , \tag{15}$$

where the small system delay T_d can be neglected for the MPC approach [26]. Therefore, x_k has dimension two representing the end-effector force and its derivative. y_k is

[1] See [23], [24] for further details on discrete matrices.

the applied force and u_k is a force reference for the AOB inner loop. From (15), the x_k prediction i samples ahead, $\tilde{x}_{k+i}$, is based on u_{k-1}, y_k, $\tilde{u}_{k+i}$ and $\hat{x}_k$, where $\hat{x}_k$ is a state estimation of (15). At each sampling time k and along the prediction horizon H_p, the future control sequence $\tilde{u}_{k+i}$ is computed by minimizing a cost function W_k to keep the predicted output $\tilde{y}_{k+i}$ as close as possible to the predicted desired force $\tilde{F}_{d,k}$. Only the first element of the computed control sequence, $\tilde{u}_{k+1}$, is sent to the AOB control loop. As the prediction horizon is displaced towards the future, new output predictions $\tilde{y}_{k+i}$ and new control sequences $\tilde{u}_{k+i}$ are computed at each sampling time.

1) Model Predictive Control Strategy: The methodology of the MPC is characterized by the following strategy:

- The finite time horizon H_p defines the slot where predicted outputs $\tilde{y}_{k+i}$ should follow $\tilde{F}_{d,k}$. H_p is bigger than the G_{cl} rise time, and its length greatly influences control tracking capabilities. Extending H_p improves performance, but increases computational time.
- At each time k, based on (15), the future outputs $\tilde{y}_{k+i}$ are predicted along H_p, where $i \in [1, H_p]$. $\tilde{y}_{k+i}$ depends on $\hat{x}_k$, u_{k-1}, y_k and $\tilde{u}_{k+i}$.
- The command vector $\tilde{u}_{k+i}$ ($i \in [0, H_p-1]$) is computed to minimize the cost function W_k, which is a quadratic function of the predicted errors between $\tilde{y}_{k+i}$ and $\tilde{F}_{d,k}$. W_k also includes predicted control efforts. Two diagonal matrices λ and δ are associated to control efforts and tracking errors, respectively. Increasing λ w.r.t. δ has the effect of reducing control activity, entailing slow response to disturbances. Decreasing λ w.r.t. δ increases control dynamics and tracking performance. Therefore, the relation between λ and δ defines the aggressiveness of the controller in recovering from disturbances [26].
- A control horizon $H_u \leq H_p$ is introduced to reduce computation time. H_u defines the time slot along which the control command $\tilde{u}_{k+i}$ is active (for $H_u \leq i < H_p$, $\tilde{u}_{k+i}$ is kept constant). Although $H_u = 1$ has acceptable performance for stable plants, increasing H_u makes the control more active up to a limit where any further increase in H_u has little effect. For high-performance a larger value of H_u is desirable. When H_u and H_p approach infinity, the prediction controller becomes the well-known linear quadratic regulator (LQR) problem [27].
- Once $\tilde{u}_{k+i}$ has been computed, only the first element $\tilde{u}_{k+i|i=0}$ is applied to system. The whole cycle of output measurement y_k, output predictions $\tilde{y}_{k+i}$, and control sequence $\tilde{u}_{k+i}$ computation is repeated and updated at each sampling time.

Since the desired force is not know in advance, $\tilde{F}_{d,k}$ is constant during the entire time horizon H_p and equal to the desired force known at instant k. The MPC control signals $\tilde{u}_{k+i}$ are computed based on the system model and cost function W_k. A good control performance can be achieved with $H_u < H_p$, entailing good tracking capabilities between F_d and y_k.

2) Formulation of MPC: From (15) and defining

$$\tilde{u}_k = \Delta\tilde{u}_k + u_{k-1} \tag{16}$$

we obtain the following state predictions,

$$\tilde{X}_k = \underbrace{\Psi\hat{x}_k + \Upsilon u_{k-1}}_{\text{past}} + \underbrace{\Theta\,\Delta\tilde{U}_k}_{\text{future}}, \tag{17}$$

with

$$\tilde{X}_k = \begin{bmatrix} \tilde{x}_{k+1} & \cdots & \tilde{x}_{k+i} & \cdots & \tilde{x}_{k+H_p} \end{bmatrix}^T, \tag{18}$$

$$\Delta\tilde{U}_k = \begin{bmatrix} \Delta\tilde{u}_k & \cdots & \Delta\tilde{u}_{k+H_u-1} \end{bmatrix}^T, \tag{19}$$

$$\Psi = \begin{bmatrix} A & \cdots & A^{H_u} & A^{H_u+1} & \cdots & A^{H_p} \end{bmatrix}^T, \tag{20}$$

$$\Upsilon = \begin{bmatrix} B \\ \vdots \\ \sum_{i=0}^{H_u-1} A^iB \\ \sum_{i=0}^{H_u} A^iB \\ \vdots \\ \sum_{i=0}^{H_p-1} A^iB \end{bmatrix} \tag{21}$$

and

$$\Theta = \begin{bmatrix} B & \cdots & 0 \\ AB+B & \cdots & 0 \\ \vdots & \ddots & \vdots \\ \sum_{i=0}^{H_u-1} A^iB & \cdots & B \\ \sum_{i=0}^{H_u} A^iB & \cdots & AB+B \\ \vdots & \ddots & \vdots \\ \sum_{i=0}^{H_p-1} A^iB & \cdots & \sum_{i=0}^{H_p-H_u} A^iB \end{bmatrix}. \tag{22}$$

Equation (17) is composed of three terms. Ψ, Υ and Θ only depend on A and B matrices, and can be computed off-line. Along the prediction horizon, the first two terms represent the *free response* and the last term is the forced one. The control increment vector $\Delta\tilde{U}_k$ is computed by minimizing the cost function

$$W_k = (\tilde{Y}_k - \tilde{F}_{d,k})^T\delta(\tilde{Y}_k - \tilde{F}_{d,k}) + \Delta\tilde{U}_k{}^T\lambda\Delta\tilde{U}_k, \tag{23}$$

with

$$\tilde{Y}_k = \begin{bmatrix} C\tilde{x}_{k+1} & \cdots & C\tilde{x}_{k+i} & \cdots & C\tilde{x}_{k+H_p} \end{bmatrix}^T, \tag{24}$$

and

$$\tilde{F}_{d,k} = \begin{bmatrix} F_{d,k} & \cdots & F_{d,k} & \cdots & F_{d,k} \end{bmatrix}^T. \tag{25}$$

Defining the prediction error $\tilde{E}_k$ as the difference between $\tilde{F}_{d,k}$ and the *free response* of the system,

$$\tilde{E}_k = \tilde{F}_{d,k} - \mathrm{diag}(C)\left[\Psi\hat{x}_k + \Upsilon u_{k-1}\right], \tag{26}$$

the cost function (23) can be written as

$$W_k = (\Theta\Delta\tilde{U}_k - \tilde{E}_k)^T\delta(\Theta\Delta\tilde{U}_k - \tilde{E}_k) + \Delta\tilde{U}_k{}^T\lambda\Delta\tilde{U}_k\,. \tag{27}$$

Developing (27), computing the gr we obtain

$$W_k = \tilde{E}_k^T\delta\tilde{E}_k - 2\Delta\tilde{U}_k{}^T\Theta^T\delta\tilde{E}_k + \Delta\tilde{U}_k{}^T(\Theta^T\delta\Theta + \lambda)\Delta\tilde{U}_k\,. \tag{28}$$

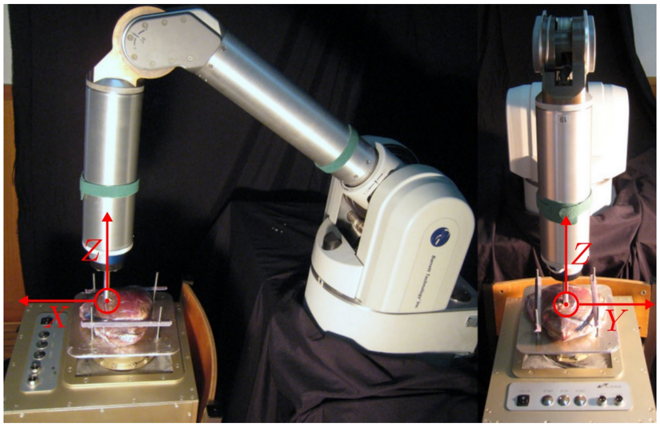

Fig. 2. Two views of the experimental setup. A lightweight 4-DoF WAM robot from Barrett Technology equipped with a 6-DoF JR3 force sensor interacts with a 3-DoF robot (called Heartbox) that generates 3D beating heart motion. An *ex vivo* heart is attached to the Heartbox and used as target for the WAM robot.

Developing (27), computing the gradient and set it to zero, we obtain the optimal and unique solution $\Delta\tilde{U}_k$ equal to

$$\Delta\tilde{U}_k = (\Theta^T\delta\Theta + \lambda)^{-1}\Theta^T\delta\tilde{E}_k\,. \tag{29}$$

Imposing $\delta \geq 0$ and $\lambda > 0$ assures that the Hessian of (27) is a positive-definite matrix, which is enough to guarantee that (29) is a minimum. According to the MPC strategy previously described, the first element $\Delta\tilde{u}_{k+i|i=0}$ of the optimal increment sequence (29) is added to the previous command u_{k-1} and sent to the AOB control loop as u_k. All the computation is repeated at each sampling time.

IV. Experimental Results

This section presents experimental results based on heart motion compensation capabilities and heart stiffness mismatches. The robotic platform used in the experiments is presented in Fig. 2. It is composed by a lightweight 4-DoF WAM robot used as a tool holder, a Heartbox and a 6-DoF JR3 force sensor (only the 3D Cartesian force is measured and filtered by a Kalman filter). The Heartbox is a 3-DoF robot used to reproduce 3D heart motion, where objects can be attached and used as targets. The cascade MPC-AOB controller described in Sections III-A, III-B and III-C is implemented on a 2.1 GHz Intel Core 2 processor running Xenomai-Linux. The communication to the WAM robot is performed by CAN bus. Integrity of the WAM robot is checked through protection functions, such as maximum joint velocity, maximum joint torque, workspace limitation and maximum forces. The control sampling time T_s is set to 1 [ms].

A two-step procedure is used to tune AOB and MPC parameters. In the first step, the AOB controller is designed to guarantee a robust stable plant, assuring good force tracking performance. Then, the MPC based on the model of this stable plant, is tuned to compensate external force disturbances due to heart motion.

A. AOB Design

Critically damped behaviors are appropriate for force-based tasks, since they represent the fastest response without overshoot. For a desired contact model $\hat{K}_s = 900$ [N/m], a damping $K_2 = 10$, and a desired G_{cl} given by (10) with $T_{cl} = 3$ [ms], the following state feedback gain

$$L_r = \begin{bmatrix} 161.5 & 1.189 & 0.557 \end{bmatrix} \tag{30}$$

is obtained. This T_{cl} entails a control bandwidth of about 34 [Hz], which is more than enough to track cardiac disturbance. The stochastic parameters reflect the model reference adaptive control strategy, where the uncertainties are lumped in p_k. R_k is set to 1 and Q_k is given by (see (14))

$$Q_{x_{r,k}} = \begin{bmatrix} 10^{-12} & 0 & 0 \\ 0 & 10^{-12} & 0 \\ 0 & 0 & 10^{-12} \end{bmatrix} \tag{31}$$

and

$$Q_{p_k} = 0.5\,. \tag{32}$$

This stochastic design entails the AOB Kalman gain

$$K_{k,f} = \begin{bmatrix} 0.1236 & 8.145 & 0.662 & 0.662 \end{bmatrix}^T. \tag{33}$$

B. MPC Design

The length of the prediction horizon H_p greatly influences control tracking capabilities. Extending H_p, a more accurate system is achieved but the computational time increases. Since our control sampling time is $T_s = 1$ [ms], a good trade-off is achieved with $H_p = 30$ and $H_u = 5$. The optimal command $\Delta\tilde{u}_{k+i|i=0}$ is computed by minimizing the cost function W, with

$$\lambda = 0.1 I_u \tag{34}$$

and

$$\delta = 0.9 I_p, \tag{35}$$

where I_u and I_p are identity matrices of size H_u and H_p, respectively.

C. 3D *Physiological Motion Compensation*

Our control architecture is designed to compensate respiration and heartbeat disturbances autonomously. To evaluate compensation capabilities of the cascade MPC-AOB controller, respiration and heartbeat signals along three axes are generated by the Heartbox. They are based on physiological motion data recorded during *in vivo* experiments on a pig's heart [28]. The WAM robot applies surgical forces on the moving heart attached to the Heartbox, and the goal is to track them. Due to the soft nature of the heart, Heartbox motion seen by the WAM robot is different from the one generated by the Heartbox. Fig. 3(a) represents the force disturbance induced by beating heart motion along three axes. This disturbance is computed from WAM robot Cartesian positions and residual force measurements recorded during two experiments. WAM robot displacements with the Heartbox turned on are subtracted from those with the Heartbox turned off. These displacements divided by the estimated heart stiffness[2] 810 [N/m] are mapped into force. Then,

[2]This estimation is done off-line from force and displacement data.

adding residual forces from the experiment with Heartbox turned on leads to the force disturbance induced by the Heartbox. Making spectral analysis, we can clearly identify two main sources of disturbance: breathing and heartbeat motions (see Fig 4). The first two peaks represent respiration (0.34 [Hz] and 0.72 [Hz]), corresponding to 20 breathing cycles per minute. The last five peaks are due to heartbeats (1.25 [Hz], 2.53 [Hz], 3.78 [Hz], 5.08 [Hz] and 6.32 [Hz]), which correspond to 75 heartbeats per minute.

3D motion compensation results are shown in Fig. 3 for X, Y and Z. Blue, green and red curves in Fig 3(a) represent Heartbox motion seen by the WAM robot. The heart signals start at 5 [s] and are repeated for around 20 [s] after a one second pause. Fig 3(b) shows desired (black curve) and applied forces (blue, green and red curves). The desired force is constant and equal to 0 [N] for X and Y, and for Z it is composed by positive and negative ramps followed by a sinusoid with increasing frequency from 0.2 [Hz] to 1 [Hz]. Residual forces are presented in Figs. 3(c), 3(d) and 3(e). The peak-to-peak amplitudes are around 0.4 [N] and the root-mean-square (RMS) values are less than 0.08 [N] for all axes, which correspond to residual motion in the order of 0.1 [mm], considering a heart stiffness of 810 [N/m]. Black curves in Figs. 3(c), 3(d) and 3(e) represent residual forces with the Heartbox turned off.

D. Robustness

The heart surface is composed by different tissues, such as fat, muscle, and arteries. During surgery the surgeon may interact not only with these tissues but also with surgical tools. Typical stiffness values for fat tissues are 300 [N/m]. The cardiac muscle (myocardium) ranges from 600 [N/m] to 1200 [N/m], and surgical tools (e.g., needle, stabilizer) have more than 1600 [N/m]. Our cascade MPC-AOB control architecture requires an approximate knowledge of the environment stiffness (see $\hat{K}_s$ in (6)). We chose to set $\hat{K}_s =$ 900 [N/m], which is the typical value of the myocardium stiffness. To assess robustness of the controller, the heart attached to the Heartbox is replaced by other objects, such as pillow and sponge. Off-line analysis have shown that pillow, heart and sponge stiffnesses are 375 [N/m], 810 [N/m] and 1900 [N/m], respectively.

Table I shows experimental results for stiffness mismatches under physiological motion for 3D constant force references (0 [N] for X and Y, and -5.0 [N] for Z). Peak to peak amplitudes of the residual forces and corresponding RMS values are not too affected by stiffness mismatches.

V. Conclusions

This paper has presented a robot control architecture for beating heart surgery relying on force feedback. We have proposed an architecture where model predictive control (MPC) drives an active observer (AOB) for autonomous heart motion compensation. This cascade MPC-AOB controller has two loops. The AOB inner-loop imposes a desired and stable closed-loop dynamics, based on non-linear feedback

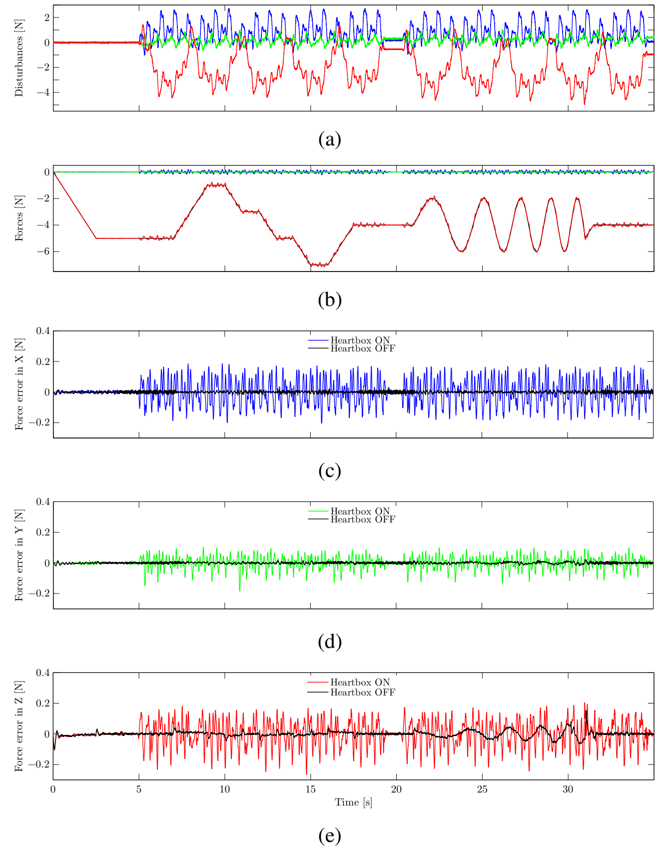

Fig. 3. MPC-AOB experimental results for 3D heart motion compensation. X, Y and Z directions are represented by blue, green and red curves, respectively. (a) Represents force disturbances induced by beating heart motion. (b) Shows desired (black curves) and applied forces (colored curves). (c), (d) and (e) Depict residual forces with the Heartbox turned on and off.

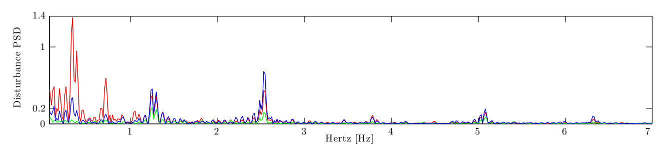

Fig. 4. Power spectral density analysis of the disturbance seen by the WAM robot and induced by beating heart motion. X, Y and Z directions are represented by blue, green and red curves, respectively.

TABLE I

Residual Forces under Stiffness Mismatches

		Pillow (375 [N/m])	Heart (810 [N/m])	Foam (1900 [N/m])
X	*peak-to-peak [N]*	0.39	0.38	0.39
	RMS [N]	0.08	0.08	0.07
Y	*peak-to-peak [N]*	0.34	0.35	0.35
	RMS [N]	0.06	0.06	0.05
Z	*peak-to-peak [N]*	0.51	0.44	0.39
	RMS [N]	0.09	0.08	0.08

linearization, augmented state-feedback, and stochastic design. The MPC outer loop generates force references for AOB control by predicting the applied force in a finite time horizon. The MPC algorithm requires knowledge of the inner-loop model, as well as desired and measured forces. A 3-DoF Heartbox robot equipped with an *ex vivo* heart generates 3D heart motion, which has been recorded during *in vivo* experiments on a pig's heart. To test our MPC-AOB control architecture, a 4-DoF WAM robot with a force sensor at the tip applies controlled surgical forces on the moving heart. Heart motion compensation capabilities, surgical force tracking and robustness to stiffness mismatches have been evaluated through *ex vivo* experiments. High quality results have been achieved. Residual peak-to-peak forces smaller than 0.5 [N] have been attained without knowing *a priori* complex and chaotic heart motion. Additionally, robustness analysis has been performed for several stiffness mismatches in the presence of heart motion (by using sponge and pillow as targets), showing good force tracking performance. The proposed MPC-AOB control architecture has been compared with stand alone AOB and MPC ones showing merits of the MPC-AOB approach. Well structured surgical tasks (like knot tying, or biopsy) can potentially benefit from MPC approaches since force references can be estimated from previous surgeries. However, even without knowing in advance force references, we show in this paper that by making MPC computations with the current surgical force reference, the MPC-AOB control performance is quite interesting.

ACKNOWLEDGMENTS

This work was supported in part by the Portuguese Science and Technology Foundation project PTDC/EEA-CRO/110008/2009. This work was also supported by project "A Surgery and Diagnosis Assisted by Computer Using Images" (SCT/2011/02/027/4824) funded by the QREN programme "Mais Centro" with financing from FEDER.

REFERENCES

[1] WHO, "World health organization," `http://www.who.int/en/`, 2009.

[2] M. F. Newman, J. L. Kirchner, B. Phillips-Bute, V. Gaver, H. Grocott, and R. H. Jones, "Longitudinal assessment of neurocognitive function after coronary-artery bypass surgery," *The New England Journal of Medicine*, vol. 344, no. 6, pp. 395–402, February 1991.

[3] A. A. Klesius, O. Dzemali, A. Simon, P. Kleine, U. Abdel-Rahman, C. Herzog, G. Wimmer-Greinecker, and A. Moritz, "Successful treatment of deep sternal infections following open heart surgery by bilateral pectoralis major flaps," *European Journal of Cardio-thoracic Surgery*, vol. 25, pp. 218–223, 2004.

[4] K. A. Eagle and R. A. Guyton, "Acc/aha 2004 guideline update for coronary artery bypass graft surgery," American College of Cardiology/American Heart Association, Reseach Report, 2004.

[5] M. Lemma, A. Mangini, A. Redaelli, and F. Acocella, "Do cardiac stabilizers really stabilize? experimental quantitative analysis of mechanical stabilization," *Interactive CardioVascular and Thoracic Surgery*, vol. 4, pp. 222–226, June 2005.

[6] R. Dzwonczyk, C. del Rio, B. Sun, R. Michler, and M. Howie, "Devices used to expose the posterior coronary artery in opcabg surgery may cause ischemia," in *Proceedings of the 31th Bioengineering conference*, vol. 2-3, 2005, pp. 148–149.

[7] R. Ginhoux, J. Gangloff, M. de Mathelin, L. Soler, M. M. A. Sanchez, and J. Marescaux, "Active filtering of physiological motion in robotized surgery using predictive control," *IEEE Transactions on Robotics*, vol. 21, no. 1, pp. 67–79, February 2005.

[8] W. Bachta, P. Renaud, E. Laroche, A. Forgione, and J. Gangloff, "Cardiolock: an active cardiac stabilizer, first in vivo experiments using a new robotized device," *J. of Computer Aided Surgery*, vol. 13, no. 5, pp. 243–254, September 2008.

[9] ——, "Active stabilization for robotized beating heart surgery," *IEEE Transactions on Robotics*, vol. 27, no. 4, pp. 757–768, 2011.

[10] R. Richa, A. P. L. Bó, and P. Poignet, "Beating heart motion prediction for robust visual tracking," in *Proceedings of IEEE Conference on Robotics and Automation (ICRA '10)*, Anchorage, USA, 2010, pp. 4579–4584.

[11] M. Kitagawa, A. Okamura, B. Bethea, V. Gott, and W. Baumgartner, "Analysis of suture manipulation forces for teleoperation with force feedback," in *Proc. of the Int. Conf. on Medical Image Computing and Computer-Assisted Intervention (MICCAI)*, Tokyo, Japan, 2002, pp. 155–162.

[12] A. M. Okamura, "Methods for haptic feedback in teleoperated robot-assisted surgery," *Ind Rob.*, vol. 31, no. 6, pp. 499–508, 2004.

[13] C. R. Wagner, N. Stylopoulos, P. G. Jackson, and R. D. Howe, "The benefit of force feedback in surgery: Examination of blunt dissection." *Presence*, vol. 16, no. 3, pp. 252–262, 2007.

[14] B. Cagneau, N. Zemiti, D. Bellot, and G. Morel, "Physiological motion compensation in robotized surgery using force feedback control," in *Proc. of the IEEE Int. Conf. on Robotics and Automation (ICRA)*, Roma, Italy, April 2007, pp. 1881–1886.

[15] Y. Nakamura, K. Kishi, and H. Kawakami, "Heatbeat synchronization for robotic cardiac surgery," in *Proc. of the IEEE Int. Conf. on Robotics and Automation (ICRA)*, vol. 2, Seoul, Korea, May 2001, pp. 2014–2019.

[16] R. Cortesão and P. Poignet, "Motion compensation for robotic-assisted surgery with force feedback," in *Proc. of the IEEE Int. Conf. on Robotics and Automation (ICRA)*, Kobe, Japan, May 2009.

[17] S. G. Yuen, D. P. Perrin, N. V. Vasilyev, P. J. del Nido, and R. D. Howe, "Force tracking with feed-forward motion estimation for beating heart surgery," *IEEE Transactions on Robotics*, vol. 26, no. 5, pp. 888–896, 2010.

[18] S. Kesner and R. Howe, "Force control of flexible catheter robots for beating heart surgery," in *Proc. of the IEEE Int. Conf. on Robotics and Automation (ICRA)*, Shanghai, China, May 2011, pp. 1589 –1594.

[19] M. Dominici, R. Cortesão, and C. Sousa, "Heart motion compensation for robotic-assisted surgery predictive approach vs. active observer," in *Proc. of the IEEE Int. Conf. on Robotics and Automation (ICRA)*, Shanghai, China, May 2011.

[20] M. Dominici, P. Poignet, and E. Dombre, "Compensation of physiological motion using linear predictive force control," in *Proc. of the IEEE Int. Conf. on Intelligent Robots and Systems (IROS)*, Nice, France, September 2008.

[21] R. Cortesão, "On kalman active observers," *Journal of Intelligent and Robotic Systems*, vol. 48, pp. 131–155, 2007.

[22] M. Dominici, P. Poignet, R. Cortesão, E. Dombre, and O. Tempier, "Compensation for 3D physiological motion in robotic-assisted surgery using a predictive force controller. experimental results," in *Proc. of the IEEE Int. Conf. on Intelligent Robots and Systems (IROS)*, St Louis, USA, September 2009.

[23] K. J. Åström and B. Wittenmark, *Computer controlled systems: theory and design*, 2nd ed. Prentice Hall, 1997.

[24] R. Cortesão, J. Park, and O. Khatib, "Real time adaptive control for haptic telemanipulation with kalman active observers," *IEEE Transactions on Robotics*, vol. 22, no. 5, pp. 987–999, October 2006.

[25] R. Cortesão, "Kalman techniques for intelligent control systems: Theory and robotic experiments," PhD thesis, University of Coimbra, Coimbra, Portugal, 2003.

[26] J. M. Maciejowski, *Predictive control with constraints*. Prentice Hall, 2002.

[27] E. F. Camacho and C. Bordons, *Model predictive control*, 1st ed. Springer-Verlag, 2004.

[28] M. Sauve, A. Noce, P. Poignet, J. Triboulet, and E. Dombre, "Three-dimensional heart motion estimation using endoscopic monocular vision system: From artificial landmarks to texture analysis," *Biomedical Signal Processing and Control*, vol. 2, no. 3, pp. 199–207, 2007.